01 Dec 2017

Estimating the Contribution of Dynamical Ejecta in the Kilonova Associated with GW170817

Benjamin P. Abbott

Marco Cavaglia
Missouri University of Science and Technology, cavagliam@mst.edu

For full list of authors, see publisher's website.

Recommended Citation

B. P. Abbott et al., "Estimating the Contribution of Dynamical Ejecta in the Kilonova Associated with GW170817," *Astrophysical Journal Letters*, vol. 850, no. 2, Institute of Physics - IOP Publishing, Dec 2017. The definitive version is available at https://doi.org/10.3847/2041-8213/aa9478

The Astrophysical Journal Letters, 850:L39 (13pp), 2017 December 1 https://doi.org/10.3847/2041-8213/aa9478

Estimating the Contribution of Dynamical Ejecta in the Kilonova Associated with GW170817

LIGO Scientific Collaboration and Virgo Collaboration
(See the end matter for the full list of authors.)

Received 2017 October 11; revised 2017 October 14; accepted 2017 October 15; published 2017 December 1

Abstract

The source of the gravitational-wave (GW) signal GW170817, very likely a binary neutron star merger, was also observed electromagnetically, providing the first multi-messenger observations of this type. The two-week-long electromagnetic (EM) counterpart had a signature indicative of an *r*-process-induced optical transient known as a kilonova. This Letter examines how the mass of the dynamical ejecta can be estimated without a direct electromagnetic observation of the kilonova, using GW measurements and a phenomenological model calibrated to numerical simulations of mergers with dynamical ejecta. Specifically, we apply the model to the binary masses inferred from the GW measurements, and use the resulting mass of the dynamical ejecta to estimate its contribution (without the effects of wind ejecta) to the corresponding kilonova light curves from various models. The distributions of dynamical ejecta mass range between $M_{\rm ej} = 10^{-3} - 10^{-2}\,M_{\odot}$ for various equations of state, assuming that the neutron stars are rotating slowly. In addition, we use our estimates of the dynamical ejecta mass and the neutron star merger rates inferred from GW170817 to constrain the contribution of events like this to the *r*-process element abundance in the Galaxy when ejecta mass from post-merger winds is neglected. We find that if $\gtrsim$10% of the matter dynamically ejected from binary neutron star (BNS) mergers is converted to *r*-process elements, GW170817-like BNS mergers could fully account for the amount of *r*-process material observed in the Milky Way.

Key words: gravitational waves – methods: data analysis – stars: neutron

1. Introduction

On 2017 August 17, 12:41:04 UTC, the Laser Interferometer Gravitational-wave Observatory (LIGO)/Virgo gravitational-wave (GW) observatory network, composed of LIGO Hanford Observatory, LIGO Livingston Observatory, and Virgo, recorded GWs consistent with a binary neutron star (BNS) inspiral and merger (Abbott et al. 2017c). This signal was subsequently named GW170817.

In addition to the GW signature, the merger of a BNS system is expected to have multiple electromagnetic (EM) signatures over different timescales (Nakar 2007; Metzger & Berger 2012). The LIGO/Virgo sky localization of GW170817 (Abbott et al. 2017c) spurred an intensive multi-messenger campaign covering the whole EM spectrum to search for counterparts (see Abbott et al. 2017d for an extended list). Within hours, broadband observations—backed by archival data investigation—revealed an optical transient (Arcavi et al. 2017; Coulter et al. 2017; Lipunov et al. 2017; Pian et al. 2017; Soares-Santos et al. 2017; Tanvir et al. 2017; Valenti et al. 2017), a type of transient called a kilonova (Li & Paczynski 1998; Metzger 2017) originating from neutron-rich matter unbound from the system (e.g., Evans et al. 2017; McCully et al. 2017; Smartt et al. 2017; Troja et al. 2017).

Broadly, two types of ejecta are expected to contribute to kilonovae: dynamical ejecta produced at the time of the merger (Rosswog et al. 1999; Metzger et al. 2010; Roberts et al. 2011; Barnes & Kasen 2013; Bauswein et al. 2013; Hotokezaka et al. 2013; Rosswog 2013; Tanaka & Hotokezaka 2013; Bovard et al. 2017; Dietrich & Ujevic 2017; Dietrich et al. 2017b; Radice et al. 2016; Sekiguchi et al. 2016), and post-merger winds produced by the remnant system, for example from an accretion disk around a black hole or massive neutron star (Dessart et al. 2009; Perego et al. 2014; Fernández et al. 2015; Kasen et al. 2015; Kiuchi et al. 2015; Martin et al. 2015; Foucart et al. 2016; Ciolfi et al. 2017; Fujibayashi et al. 2017; Shibata et al. 2017; Siegel & Metzger 2017).

Both EM and GW measurements rely on models to connect the underlying properties and composition of the ejecta to their respective observations. The process of interpreting ejecta based on EM observations is described in Alexander et al. (2017), Arcavi et al. (2017), Chornock et al. (2017), Covino et al. (2017), Cowperthwaite et al. (2017), Diaz et al. (2017), Drout et al. (2017), Evans et al. (2017), Kasen et al. (2017), McCully et al. (2017), Nicholl et al. (2017), Pian et al. (2017), Smartt et al. (2017), Tanaka et al. (2017), Troja et al. (2017), and Abbott et al. (2017d). We use phenomenological calculations that estimate the dynamical ejecta mass from the pre-coalescence binary properties, which GW observations can constrain. This mass is a critical ingredient needed to predict the contribution of dynamical ejecta to the EM light curve associated with this kilonova transient. Going forward, this procedure would also assist in the interpretation of future follow-up observations where a dim counterpart was detected, or none at all.

This Letter shows how dynamical ejecta masses obtained from GW parameter estimates of GW170817 via phenomenological fits to numerical models for the mass and velocity of dynamically ejected matter in BNS systems (Dietrich & Ujevic 2017, hereafter DU17) can predict kilonova light curves.

Similar numerical work has produced fitting formulae in the case of neutron-star black-hole (NSBH) binaries (Kawaguchi et al. 2016). While the GW detection of GW170817 cannot rule out the presence of a black-hole companion, the BNS interpretation is favored (Abbott et al. 2017c). Consequently, we do not include the NSBH scenario in this work, and only employ the fitting formulas for ejecta mass and velocity from BNS simulations (DU17). The GW170817 analysis extracted the BNS source parameters using Bayesian inference (Abbott et al. 2017c), and those results are used here to estimate the mass of the dynamical ejecta. This approach accounts for the dependence of the amount of ejected matter on the size and stiffness (Kawaguchi et al. 2016) of the components of the binary, characterized by the equation of state (EOS) and its influence on the mass–radius relationship (Lattimer & Prakash 2001; Özel & Freire 2016).

Bayesian inference with a GW signal model applied to the strain data provides a posterior distribution of component masses (m_i) and dimensionless spins ($\chi_i \equiv c|\boldsymbol{S}_i|/(Gm_i^2)$, where $\boldsymbol{S}$ is the angular momentum of the neutron star (NS)) consistent with the observations (Veitch et al. 2015). Assuming NS spins are small ($\chi \leqslant 0.05$, hereafter "low-spin"), we obtain distributions of ejecta between 10^{-3} and $10^{-2}\,M_\odot$. Allowing for larger NS spins ($\chi \leqslant 0.89$, hereafter "high-spin") pushes some ejecta values higher, of the order of $10^{-1}\,M_\odot$ at its highest. In this Letter, we focus on dynamical sources, so it is important to recall that this analysis may not account for a significant fraction of the ejecta mass; winds could produce comparable or even more ejecta than from dynamical sources. Using the GW-derived dynamical ejecta estimates, the derived light curves vary significantly between the adopted models, in both color evolution and time and magnitude of peak emission; in extreme cases, they can reach beyond 15th magnitude in optical bands.

Like supernovae (Terasawa et al. 2001), neutron star mergers are believed to contribute to the abundance of heavy elements (Lattimer & Schramm 1974) through r-process nucleosynthesis (Burbidge 1954). Using our GW estimates of dynamical ejecta masses and the merger rates inferred from the BNS discovery (1540^{+3200}_{-1220} Gpc^{-3} yr^{-1}; Abbott et al. 2017c), we estimate a present-day r-process density of $10^{1.7}$–$10^{3.2}\,M_\odot$ Mpc^{-3} contributed by BNS mergers. Under the assumption that all BNS mergers produce the same amount of dynamical ejecta that we infer for GW170817, this estimate is consistent with the Galactic values and suggests that the associated nucleosynthesis is one of the primary contributors to r-process abundances.

2. Predicted Dynamical Ejecta Mass

In general, the amount of ejecta from binary mergers depends on the masses and EOS of the two components, their rotation, and, most importantly for post-merger winds, the neutrino/radiation hydrodynamics and the magnetic fields, e.g., Hotokezaka et al. (2013), Martin et al. (2015), Dietrich et al. (2017b), Radice et al. (2016), Sekiguchi et al. (2016), and Siegel & Metzger (2017). Based on detailed numerical studies of merging, irrotational binaries, the phenomenological fits devised by DU17 relate the dynamical ejecta mass $M_{\rm ej}$ to the gravitational mass of the component stars (m), their baryonic mass (m_b), and their radii R (or equivalently compactnesses $C = Gm/Rc^2$). Contributions due to winds were not included in the simulations used by DU17, and thus are not part of the fits for $M_{\rm ej}$, even though they may lead to comparable ejecta masses.

Because the EOS in neutron stars is poorly constrained, two approaches are taken to describe the bulk properties of the binary components. In the first approach, we assume an EOS and infer m_b and C from the binary's measured gravitational masses using a zero-temperature non-rotating model (computed using the Oppenheimer–Volkoff equations, Oppenheimer & Volkoff 1939). Different EOSs will predict different radii and baryonic masses for the same gravitational masses and, as such, will affect the amount of ejecta and the predicted light curve of the kilonova. The EOS of cold, dense, degenerate matter is poorly constrained (see Oertel et al. 2017 for a recent review), so we evaluate a representative selection of the EOS considered in Özel & Freire (2016). The tidal deformabilities allowed by GW170817 (Abbott et al. 2017c) do disfavor stiffer EOSs; however, many remain compatible with our measurements. Due to observational constraints, we restrict ourselves to EOSs that have a maximum mass above $1.97\,M_\odot$ (Demorest et al. 2010; Antoniadis et al. 2013). Specifically, we consider EOS calculations from Glendenning (1985, GNH3), Müther et al. (1987; MPA1), Wiringa et al. (1988; WFF1-2), Engvik et al. (1996; ENG), Müller & Serot (1996; MS1, MS1b), Akmal et al. (1998; APR3-4), Douchin & Haensel (2001; SLy), and Lackey et al. (2006; H4).

In the second case, we take an approach that does not assume a specific EOS to compare against our EOS-specific results. The internal structure of the NSs in a binary is encoded in the gravitational waveform through the (dimensionless) tidal deformabilities (denoted Λ) of the NSs (Flanagan & Hinderer 2008; Damour et al. 2012; Del Pozzo et al. 2013; Wade et al. 2014). One can infer m_b and C from the binary's measured gravitational masses and tidal deformabilities by applying fits from Coughlin et al. (2017) and Yagi & Yunes (2017), which give $m_b(m, C)$ and $C(\Lambda)$, respectively. While some error is incurred using these additional fits, it is small compared to the estimated uncertainty of the fits for the dynamical ejecta properties and the intrinsic uncertainty in current numerical relativity simulations. Specifically, for the EOS considered by Yagi & Yunes (2017), the error in the tidal deformability-compactness relation is $<10\%$ for the nuclear EOS, while for the baryonic mass fit, the maximum error found by Coughlin et al. (2017) is $<3\%$. When applying these fits, we also exclude cases with component masses above $3\,M_\odot$, a standard upper bound on NS masses (Kalogera & Baym 1996), and restrict the compactness to be below the Buchdahl bound (Buchdahl 1959) of $4/9 \simeq 0.44$, which similarly only affects a few cases.

2.1. Sources of Uncertainties in Ejecta Mass Estimation

Many caveats must be considered when assessing the uncertainty in estimates of $M_{\rm ej}$. The amount of ejecta from mergers also depends on various microphysics, such as the particular treatment of thermal effects, neutrino transport, and magnetic fields (Dessart et al. 2009; Bauswein et al. 2013; Perego et al. 2014; Radice et al. 2016; Sekiguchi et al. 2016; Bovard et al. 2017; Ciolfi et al. 2017), which lead to uncertainties about the ejecta's structure, angular distribution, and composition (Kasen et al. 2013; Tanaka & Hotokezaka 2013; Barnes et al. 2016). These parameters are not included in the $M_{\rm ej}$ fits in DU17. Additionally, the DU17 fits ignore the effects of spin on dynamical ejecta, which can change the amount of ejecta (Kastaun & Galeazzi 2015; Dietrich et al. 2017a; Kastaun et al. 2017). In particular, aligned spin can

increase torque in the tidal tail and lead to more ejecta, which is most notable for unequal mass configurations. To understand the effect of spin on dynamical ejecta, additional better resolved simulations are needed.

Systematic uncertainties are also of concern. The accuracy of the $M_{\rm ej}$ fit from DU17 relies on the underlying numerical relativity simulations. Simulation choices for input physics (nuclear EOS and microphysics), inclusion of different neutrino transport models, and chosen grid resolution can all result in large systematics. For example, comparisons of numerical relativity predictions of $M_{\rm ej}$ differ by a factor of $\sim$4 (Lehner et al. 2016; Sekiguchi et al. 2016; Bovard et al. 2017). Further, the error on ejecta masses from numerical simulations likely has an absolute component, leading to increasing relative errors for low ejecta masses—for additional discussion see Endrizzi et al. (2016) and Ciolfi et al. (2017). An error at low masses is not symmetric as $M_{\rm ej}$ cannot be negative, potentially biasing the phenomenological fits of DU17 to an overestimation of the ejecta mass. Additionally, there are also systematic uncertainties introduced by the specific form of the fit, where all EOS effects are contained in the values of m_b and C for a given m. Finally, as discussed in Abbott et al. (2017c) and Section 2.2, the waveform model used to infer the masses and tidal deformabilities from the GW signal introduces its own systematic uncertainties, though these are estimated to be smaller than those of the DU17 $M_{\rm ej}$ fit.

All of these considerations contribute to the uncertainty in the $M_{\rm ej}$ fit from DU17; the error is a mixture of systematic errors that need investigation with dedicated future studies and numerical simulations. To model some part of this error, we will treat the average relative error of the fit quoted in DU17 (72%) as a statistical error for any results used here, and defer a more robust error analysis to future work. We include an estimate of the error of the $M_{\rm ej}$ fit from DU17 by replacing each ejecta mass sample with a random value consistent with a Gaussian distribution in $\log_{10} M_{\rm ej}$ centered on the value and with standard deviation of $\log_{10} 1.72$, as motivated in Section 2.1. This method excludes zero ejecta masses, and errors for small ejecta masses $\lesssim 10^{-3}\,M_\odot$ are not well modeled. The ejecta mass fit is based on simulations with nonzero ejecta mass. The full parameter space likely also contains cases with little or no ejecta mass, for example, systems exhibiting prompt black-hole formation. Since we reported in Abbott et al. (2017b) that prompt collapse can only be excluded for extreme EOSs such as MS1, and the fit at values below $3 \times 10^{-3}\,M_\odot$ strongly overestimates the ejecta mass compared to the numerical relativity (NR) data points, the fit cannot reliably exclude zero ejecta mass below this value. Figure 1 shows that, in the low-spin cases, the number of samples less than $M_{\rm ej} < 3 \times 10^{-3}\,M_\odot$ is typically $\sim$10%–15% of the cumulative total for most. In extreme cases, this fraction is up to 50%, but also arises from EOSs that have been disfavored in Abbott et al. (2017c). In the high-spin cases, this number is typically smaller, around 5%–10%, but can reach up to 25% in the extreme cases. We also discard the few samples where the fit predicts a negative value.

2.2. Ejecta Mass Predictions

We evaluate the $M_{\rm ej}$ fit using the binary parameters derived from the GW analysis (Abbott et al. 2017c). These parameters include the gravitational masses, tidal deformabilities, and spins of the component stars, though the spins are not used in evaluating the fit. Bayesian inference provides a distribution of these parameter values as a set of independent samples drawn from the posterior (Veitch et al. 2015; Abbott et al. 2016a). As a quantity that derives from these binary parameters, $M_{\rm ej}$ then is also represented as a statistical sample.

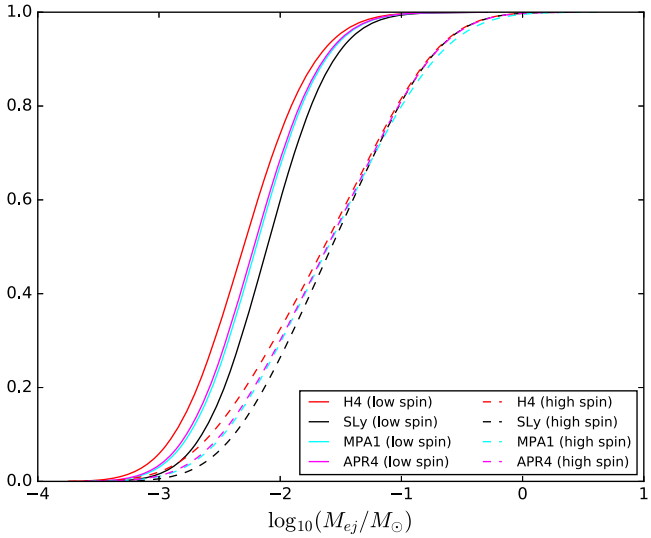

Figure 1. The figure above displays the cumulative distribution function of the dynamical ejecta mass predicted for a representative selection of the EOS in the study. The low-spin cases are traced in solid colors and the high-spin case are dashed curves.

While the estimation of $M_{\rm ej}$ does not include the component spins as an input, they are an important degree of freedom in the waveform models used in the GW analysis. We consider two sets of GW parameter samples, defined by the choices for the prior on the spin magnitude. The two spin priors considered here are $\chi \leqslant 0.89$ (our "high-spin" case with the upper limit dictated by the waveform model used), and $\chi \leqslant 0.05$ (our "low-spin" case, slightly above the largest inferred spin at the merger of an NS in a BNS system that will merge within a Hubble time (Burgay et al. 2003)). While the waveform models used only include the effects of the spin components along the orbital angular momentum, the spin priors assume isotropic spin directions. The very highest spins allowed in the high-spin posterior set exceed the mass-shedding limit ($\chi \sim 0.7$ for the EOS considered in Lo & Lin 2011), but the small density of posterior samples in this region lies outside the 90% credible intervals. More importantly, the high-spin posterior on the primary mass contains samples with masses well above the maximum mass allowed for a static NS for any of the EOSs we consider; we simply exclude from consideration any samples with such unsupported masses for each EOS.

There are also systematic errors introduced by the waveform model used. As discussed in Abbott et al. (2017c), analysis with a different waveform model changes the 90% credible bounds on the masses by $\sim$15% in the high-spin case (with no changes in the low-spin case), and the bounds on the tidal deformabilities by $\sim$20%–30% in both low- and high-spin cases. As these differences are below the systematic errors of the DU17 fit, we do not attempt to account for them here. The true systematic errors from waveform models may be significantly larger than those estimated in this comparison; making such assessments is the subject of future work.

Figure 1 reports cumulative probability distributions for the dynamical ejecta for a selection of the EOS tested. While all of

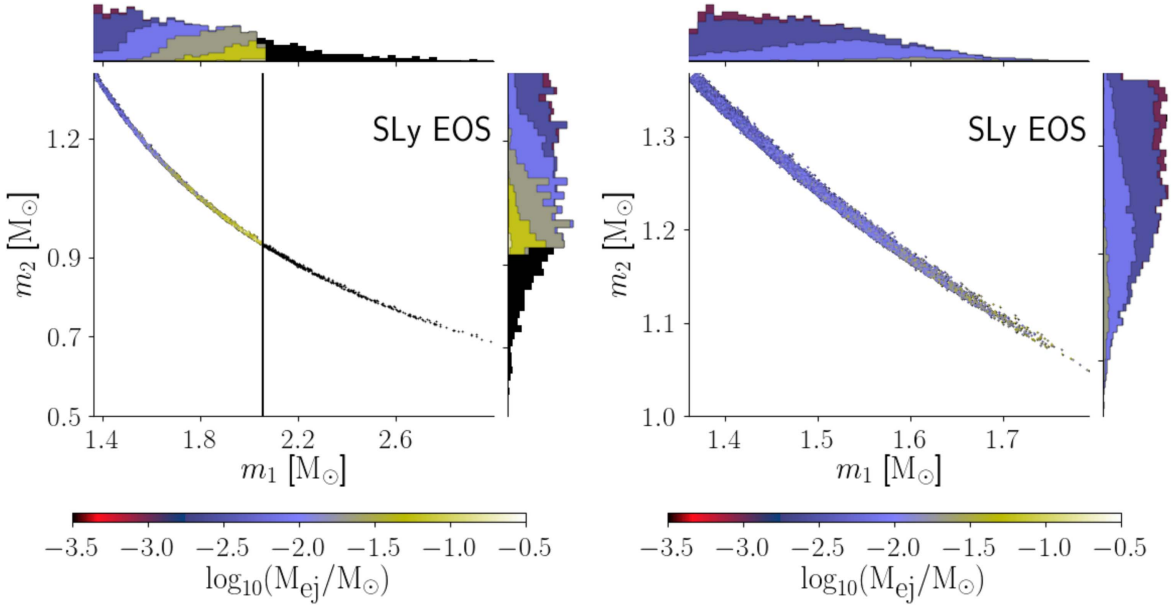

Figure 2. The left (high-spin prior) and right (low-spin prior) panels above show the distribution of the primary (m_1) and secondary (m_2) masses from GW measurements. The color of each point indicates the predicted dynamical ejecta mass for each sample that the SLy EOS allows. In the left-hand plot, black markers correspond to m_1 values that are disallowed by the maximum mass of the EOS (marked by a vertical line). The underlying black histograms to the top and right of each plot are the one-dimensional marginalized histograms of the masses. The stacked histograms on top of them in various colors show the binary masses that create ejecta masses above logarithmically spaced thresholds of 1×10^{-3}, 3×10^{-3}, 8×10^{-3}, 2×10^{-2}, 6×10^{-2}, and $2 \times 10^{-1}\,M_\odot$, where only the first four are nonzero in the right-hand plot.

the cases predict ejecta concentrated between 10^{-3} and $10^{-2}\,M_\odot$, the high-spin results allow for larger median ejecta values in general—maximum values can exceed a tenth of a solar mass. Since the DU17 fits for M_{ej} neglect spin, the differences in ejecta for the cases shown in Figure 1 are driven by the imprint of the spin choices inherent in the GW analysis that was input into this analysis.

Figure 2 shows the distribution of ejecta masses using the SLy EOS, illustrating how the ejecta mass tends to scale with the component mass distribution. Among the EOSs tested, SLy is closer to the lower side of ejecta distributions in both the estimated median and maximum ejecta. The fits themselves imply an ejecta distribution strongly dependent on the mass of the primary (m_1) and the difference between the primary and secondary masses. However, applying the fit uncertainty smears the ejecta distribution over the difference of the component masses. This effect is most evident in the marginal distributions plotted as histograms on the sides of the Figure 2 panels. Since the high-spin distribution has more posterior samples away from equal mass systems, as well as larger primary masses overall, more samples give rise to larger ejecta masses. While this only affects the high-spin case, those EOSs that allow for larger maximum masses also allow for a larger maximum ejecta values, typically $M_{ej} > 10^{-1}\,M_\odot$ (above the maximum ejecta mass of $6.5 \times 10^{-2}\,M_\odot$ in the simulations to which the M_{ej} fit has been calibrated). This is a natural consequence of larger maximum masses corresponding to larger differences between m_1 and m_2, as illustrated in Figure 2.

3. Kilonova Light Curve Models

Current kilonova emission models (Li & Paczynski 1998; Barnes et al. 2016; Metzger 2017; Tanaka et al. 2017) produce spectral energy distributions between the ultraviolet (UV) and the near-infrared (NIR). Generally, there are two different physical processes that require modeling. First, the conversion of dynamical and wind ejecta material into *r*-process elements (i.e., the nucleosynthesis; Kasen et al. 2013, 2015; Barnes et al. 2016; Metzger 2017; Rosswog et al. 2017), and second, the production of an associated EM transient (Metzger et al. 2010; Kasen et al. 2013; Barnes et al. 2016; Rosswog et al. 2017). Beyond these considerations, there are still several important nuclear physics ingredients that are unknown, such as opacity and heating rate, and can lead to large uncertainties in light curve prediction (see, e.g., Rosswog et al. 2017). We do not attempt to model these uncertainties.

We briefly describe here three parameterized models used to generate light curves in this work. Wollaeger et al. (2017) use radiative transfer simulations and provide analytic fits for the peak time, bolometric luminosity, and color corrections as a function of ejecta parameters. The Wollaeger et al. (2017) light curves are scaled as a function of ejecta mass and velocity, which changes both the time of peak luminosity as well as peak magnitude. We obtain the velocity from additional fits in DU17, and assume an opacity of $10\,\mathrm{cm^2\,g^{-1}}$, thus modeling the presences of lanthanides. Conversely, Metzger (2017) provide a toy model for blue kilonova with opacity $0.1\,\mathrm{cm^2\,g^{-1}}$ for lanthanide-free matter. DU17 use the radiative Monte-Carlo (MC) simulations of Tanaka & Hotokezaka (2013) and derive an analytical model for kilonova emission driven by dynamical ejecta from a BNS merger. No wind contribution is included in DU17, although winds can potentially dominate (Kiuchi et al. 2015; Ciolfi et al. 2017; Siegel & Metzger 2017). The dynamical ejecta models tend to predict redder and more slowly rising NIR than wind-driven models.

Light curves from dynamical ejecta models depend significantly on the thermalization efficiency, the radiation transport simulations used, and other assumptions (Metzger & Fernandez 2014; Coughlin et al. 2017; Rosswog et al. 2017). In our analysis we do not consider observational error from

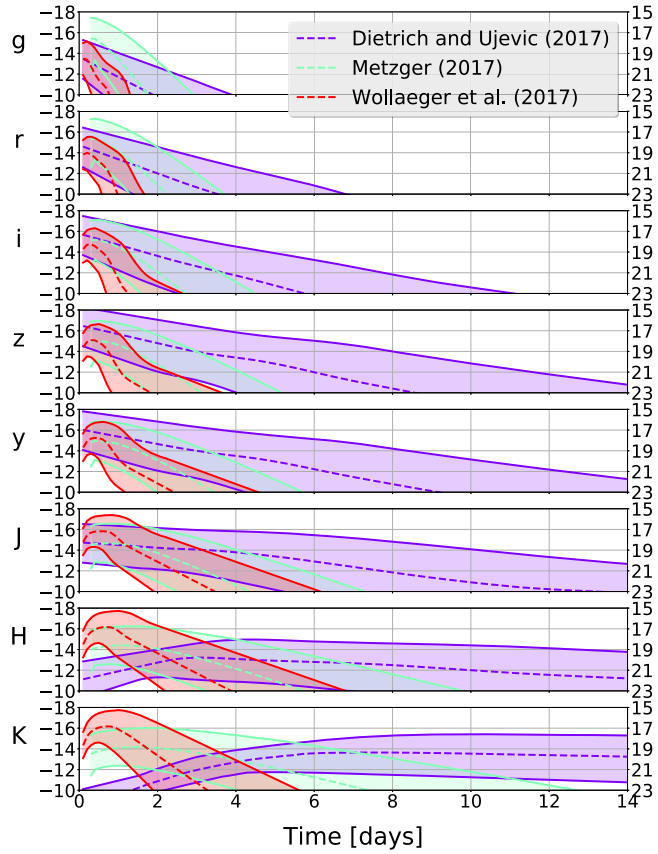

Figure 3. Absolute (left vertical axis) and apparent (right vertical axis) magnitudes of light curves consistent with parameter estimation for astrophysical spins for the kilonova models of DU17, Metzger (2017), Wollaeger et al. (2017) in *grizyJHK* filters. In particular, the DZ2 model is employed from Wollaeger et al. (2017). The dashed lines show the median light curve, while the shaded intervals show the 90% intervals. In addition to including the average relative error (72%) of the ejecta-mass fitting formula, we include 1 mag errors on the intervals to account for errors in the models themselves (Coughlin et al. 2017). The lower percentiles are not conservative as we cannot definitively exclude zero ejecta mass due to unmodeled systematics. The fiducial distance to the event is 40 Mpc.

extinction in the light curve prediction, as it is likely smaller than the systematic error of the models (Kawaguchi et al. 2016).

4. Predicted Kilonova Light Curves

In conjunction with the mass and tidal estimates for the low-spin case, we calculate the mass and velocity of dynamical ejecta as described in Section 2. Using the light curve models of DU17, Metzger (2017), and Wollaeger et al. (2017), we show the absolute and apparent magnitudes consistent with these estimates of dynamical ejecta in Figure 3. Here, we employ the DZ2 model from Wollaeger et al. (2017), and set 40 Mpc (near the median of the GW distance posterior (Abbott et al. 2017a, 2017c)) as the fiducial distance to the event for calculating the apparent magnitudes. DU17 exhibits the features of most lanthanide-rich dynamical ejecta models, with a rapid fade in the blue and a late rise in the NIR. Wollaeger et al. (2017), which also considers the contribution from the wind ejecta of 0.005 $M_{\odot}$, is brighter, has a slower fade in the blue, and a faster fade in the NIR. The model in Metzger (2017) —adopted here only considering dynamical ejecta—is between these two models, originally brighter in the blue and NIR bands

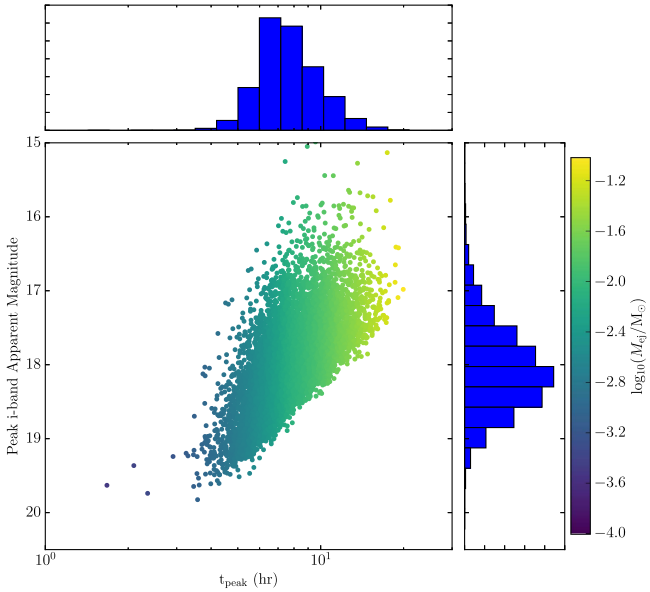

Figure 4. Inferred peak *i*-band apparent magnitude vs. time of peak *i*-band magnitude with the blue model in Metzger (2017) and low-spin sample distribution (marginal distributions on M_{ej} and time of peak shown on the top and right). Apparent magnitudes are calculated from the dynamical ejecta only, using the GW inferred distance.

(*g*, *r*, *i*, *z*) than either of these models, but fades more quickly than Wollaeger et al. (2017).

Employing the lower-opacity blue-peaked model in Metzger (2017) and GW inferred distance, we can calculate the distribution of peak times and observed peak magnitudes in a given photometric band. As the source resides at a low redshift, we neglect the cosmological redshift of the source. Figure 4 shows the peak *i*-band magnitudes from those light curves versus the time of peak *i*-band magnitude when considering the low-spin distribution. The samples from the high-spin distribution produce the peaks that are brighter by one magnitude on average. This is understood from the ejecta distributions in Figure 2—the low-spin distribution tends to produce less ejecta and hence is less luminous. We note again that the light curves in Figure 3 are calculated with a distance fixed to the source, while the magnitudes in Figure 4 fold in the distance inferred from the GW data. Thus, a wider spread arises from the variance in the GW-only distance posterior distribution. Including the distance values from the GW posteriors provides a better estimation of the variation that would arise in a prediction from GW information alone, as opposed to having constraints from EM measurements.

The estimates presented here are a proof-of-principle study with which to illustrate what is presently possible with forward modeling from GW observations. In particular, if it is available before EM observations begin, or in a situation before a confident counterpart has been identified (e.g., due to poor sky localization), analysis driven by the GW data can inform EM follow-up observations and interpretation, particularly in cases where (due to geometric effects and observational delays) the effect of dynamical ejectas on the light curve is enhanced. Predictions of peak times in the emission and the color evolution are useful for comparison with early observations, and provide falsifiable predictions with which to evaluate models of the source.

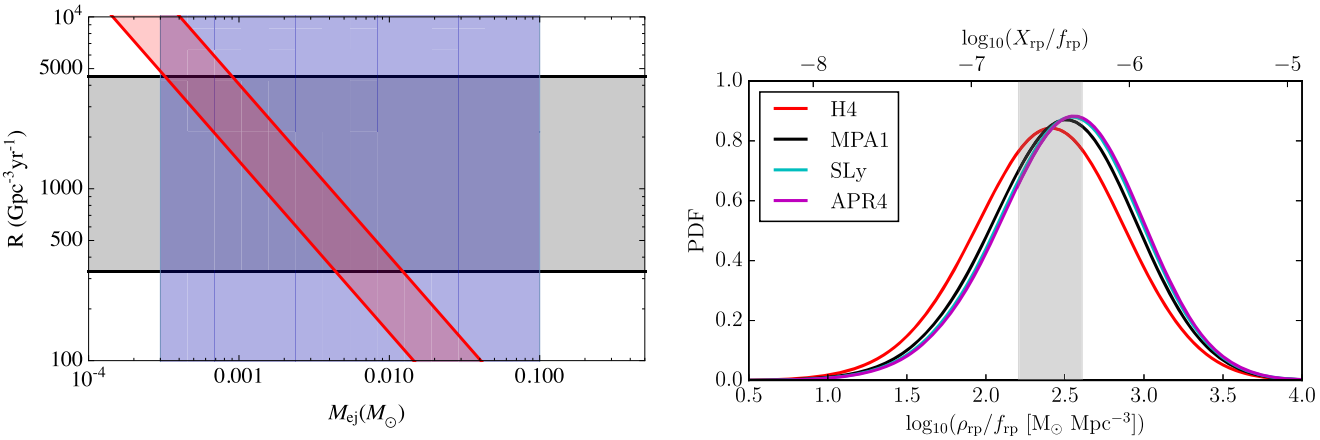

Figure 5. Left panel: plot of the present-day BNS merger rate density $\mathcal{R}$ vs. dynamical ejecta masses $M_{\rm ej}$. The solid gray band corresponds to the event rate range deduced from GW170817. The solid blue band shows the approximate range of conceivable dynamical ejecta masses, based on the ejecta models used in this work. The red band shows the approximate range of *r*-process elements per unit volume, based on Galactic observations, an approximate density of MW-like galaxies (0.01 Mpc^{-3}), a range of Galactic masses, and *r*-process formation efficiencies $f_{\rm rp}$ between 0.5 and 1. Configurations in the intersection of all three bands correspond to cases where dynamical ejecta from BNS mergers are solely responsible for *r*-process element formation. Right panel: probability distributions of *r*-process material density and abundance (normalized by $f_{\rm rp}$) from dynamical ejecta for different EOSs at $z = 0$. The lower (upper) bound on the 90% credible interval for $\rho_{\rm rp}/f_{\rm rp}$ over all EOSs is $10^{1.7}\ M_\odot$ Mpc^{-3} ($10^{3.2}\ M_\odot$ Mpc^{-3}). The vertical gray band shows the Solar *r*-process abundance (Arnould et al. 2007).

5. Abundance of *r*-process Material

The *r*-process and *s*-process are the two known mechanisms by which heavy elements can be synthesized (Burbidge et al. 1957). To assess the contribution of the *r*-process to the observed abundances of heavy elements (Arnould et al. 2007; Sneden et al. 2008), one can identify the abundances expected from the *s*-process alone, and hence the *r*-process residual. SNe II can produce *r*-process elements, but they may not produce the observed abundance patterns (e.g., Freiburghaus et al. 1999). BNS mergers could also account for these elements. However, quantifying the contribution of those mergers has remained elusive due to poor constraints on both the rate of mergers as well as the amount of matter ejected in each merger. With GW170817, we are able to constrain both of these quantities significantly from data.

If BNS mergers are to produce most of the observed *r*-process elements in the Milky Way (MW), the mergers must occur with a sufficiently high rate and eject significant amounts of *r*-process material. Assuming dynamical ejecta dominate over winds, the mass fraction $X_{\rm rp}$ of *r*-process nuclei in the MW should be proportional to the merger rate density $\mathcal{R}$ and dynamical ejecta mass $M_{\rm ej}$, with a proportionality constant set by the local galaxy density and the MW age and mass. Following Qian (2000), we estimate that the merger rate and ejecta per event are approximately related by $\mathcal{R} \simeq 600(f_{\rm rp}M_{\rm ej}/10^{-2}\,M_\odot)^{-1}$ Gpc^{-3} yr^{-1}. In this relationship, $f_{\rm rp} \equiv M_{\rm rp}/M_{\rm ej}$ is the fraction of matter dynamically ejected in NS mergers that is converted to heavy *r*-process elements rather than lighter products, e.g., α particles. The value of $f_{\rm rp}$ depends on details of the dynamics, geometry, and neutrino illumination of the ejected matter, all of which change the electron fraction (Y_e) distribution of ejected matter (see, e.g., Goriely et al. 2015; Kasen et al. 2015). However, various studies have suggested significant *r*-processing of ejecta material (e.g., Goriely et al. 2011, 2015; Wanajo et al. 2014; Just et al. 2015; Radice et al. 2016). The red band in the left panel of Figure 5 shows this relationship between $\mathcal{R}$ and $M_{\rm ej}$ for $f_{\rm rp} \in [0.5, 1]$ (e.g., Goriely et al. 2015). Also shown in the left panel are the constraints on the local rate density of BNS mergers from GW170817 (gray) and the range of ejecta masses typically considered in the literature (blue). The overlap of these constraints suggests that BNS mergers could account for all of the observed *r*-process abundance.

A more detailed calculation of *r*-process enrichment from the dynamical ejecta of BNS mergers can be done using the specific distributions of $M_{\rm ej}$ and $\mathcal{R}$ inferred from GW170817. Under the assumption that all binary mergers have the same ejecta mass as that inferred from GW170817, we calculate the average dynamically ejected local *r*-process material density according to

$$\rho_{\rm rp} = f_{\rm rp} M_{\rm ej} \mathcal{R} \frac{\int_0^{t_h}\int_0^{t} \dot{\rho}_*(\tau) p_{\rm delay}(t-\tau)\,d\tau dt}{\int_0^{t_h} \dot{\rho}_*(\tau) p_{\rm delay}(t_h-\tau)\,d\tau}, \quad (1)$$

where t_h is the Hubble time.[164]

In this expression, $\dot{\rho}_*$ is the cosmological star formation rate, assumed to follow Madau & Dickinson (2014); $p_{\rm delay}$ is the delay time distribution of NS mergers, $p_{\rm delay}(t) \propto t^{-1}$ (see, e.g., O'Shaughnessy et al. 2008; Dominik et al. 2012), with a minimum delay time of 10 Myr; and $\mathcal{R}$ is the present-day merger rate density for NS mergers. The denominator is a normalization factor that scales the present-day merger rate density to $\mathcal{R}$.

In the right panel of Figure 5, we plot the distribution of $\rho_{\rm rp}/f_{\rm rp}$ for a few representative EOSs using our $M_{\rm ej}$ distributions and the rates inferred from GW170817. On the top axis, we also show $X_{\rm rp}/f_{\rm rp} = (\rho_{\rm rp}/f_{\rm rp})/\rho_*$, where $\rho_* = \int_0^{t_h} \dot{\rho}_*(t)dt$. If $f_{\rm rp} = 1$, the range $10^{1.7}\,M_\odot$ Mpc^{-3}–$10^{3.2}\,M_\odot$ Mpc^{-3} brackets our 90% credible intervals on $\rho_{\rm rp}$ for all EOSs. Both $\rho_{\rm rp}$ and $X_{\rm rp}$ are shown normalized to $f_{\rm rp}$, *as* $f_{\rm rp}$ depends on unknown details of the merger. The gray band in the right panel of Figure 5 shows the MW mass abundance of *r*-process elements, derived from Arnould et al. (2007). As long as $f_{\rm rp} \gtrsim 10\%$ of the dynamically ejected mass is converted to heavy *r*-process elements, dynamical ejecta could account for all of the MW

[164] We assume ΛCDM cosmology with TT+lowP+lensing+ext parameters from Ade et al. (2016).

r-process abundance. We have not factored in modeling details such as the relative abundance pattern of r-process elements, the value of $f_{\rm rp}$, the relative contribution of dynamical versus wind ejecta, and uncertainties in the star formation history of the Universe.

6. Conclusions

In this Letter, we derive estimates for the dynamical ejecta mass produced by the BNS merger GW170817, as well as the corresponding kilonovae light curves and r-process nucleosynthesis yields, without additional photometric or EM spectral data. These estimates have the GW data as their foundation and use a fit to a wide variety of simulations to obtain dynamical ejecta masses from these data. Our predictions for light curves include a range of possible magnitudes and timescales of emission. In general, for the blue model in Metzger (2017) in the i-band, we predict peak magnitudes concentrated between $\sim$19 and $\sim$17 for a merger consistent with our low-spin results, and peak magnitude between $\sim$19 and $\sim$16—typically lasting twice as long—for mergers consistent with high-spin results. Such predictions can guide expectation as to whether or not future, perhaps more distant, counterparts would be observable with a given facility. The predictions from the GW inference for the dynamically unbound matter depend strongly on the allowed spin configurations in the GW model, which in turn influence the predicted light curves. The low-spin results predict smaller ejecta masses on the whole, and as such, a bright kilonova event (e.g., $>$16 magnitude) may indicate a faster spinning NS component. We stress that the phenomenological fits used to predict $M_{\rm ej}$ themselves are not corrected for spin effects, so this increased brightness occurs because of degeneracies in the GW parameter estimates between spin and mass ratio.

We have also presented predicted light curves derived from other models in the literature. Our results show that when large amounts of ejecta mass are allowed, the light curves have brighter peaks and are longer-lived. They differ in color evolution, however (compare DU17 and Wollaeger et al. 2017, for example) and EM observations combined with these curves could hint at mixtures of different ejecta material compositions (Metzger 2017). For example, strong emission observed in both blue and red bands could imply sectors of material containing both high and low electron fractions. However, the Metzger model, as implemented here, neglects post-merger wind effects, and in general, these conclusions only hold under the assumption that dynamical ejecta dominate the mass ejection.

Our results suggest that dynamical ejecta from rare NS mergers could be an important and inhomogeneous source of r-process elements in the Galaxy (Beniamini et al. 2016; Ji et al. 2016). If more than $f_{\rm rp} \gtrsim 10\%$ of the mass ejected from mergers is converted to r-process elements, our prediction for average r-process density in the local universe is consistent with the Galactic abundance. Our approach does not address the contribution from winds, which could eject a substantial overall mass but may (Siegel & Metzger 2017) or may not (Rosswog et al. 2017) have the wide range of Y_e needed to produce all r-process abundances (i.e., the second and third r-process peak). Our approach is also not as detailed as full multi-species chemical enrichment calculations used to interpret observations of individual elements in targeted populations (see, e.g., Côté et al. 2017). As Advanced LIGO and Virgo approach design sensitivity, these observational constraints should rapidly shrink, enabling more precise tests of the BNS r-process nucleosynthesis paradigm. Additionally, present and future EM observations should provide complementary information to directly constrain those parameters that our analysis cannot.

Finally, if EM measurements are consistent with a total ejecta mass (dynamical and wind) of $\gtrsim$0.01 $M_\odot$, and if we require consistency with low neutron star spins, then one possible conclusion is that winds contribute significantly to the total ejected mass. However, if winds dominate, then the dynamical ejecta mass will be an important but potentially difficult to measure component in the light curve, which our calculations can supply. Additionally, with so much material ejected per event, to be consistent with our inferred detection rate, we would predict that only a fraction of the ejecta can form r-process elements.

The coincidence of GW170817 and GRB 170817A was an exceptionally rare event, allowing for a unique set of measurements to be made about the processes driven by the BNS merger. Future observations should facilitate the refinement of these measurements. The observation of GW170817 suggests that in the upcoming year-long third observing run (Abbott et al. 2016b) with a three-instrument GW network, there will likely be more GW observations of BNSs. In the coming years, GW measurements will allow for better understanding of populations of kilonova events.

The authors gratefully acknowledge the support of the United States National Science Foundation (NSF) for the construction and operation of the LIGO Laboratory and Advanced LIGO as well as the Science and Technology Facilities Council (STFC) of the United Kingdom, the Max-Planck-Society (MPS), and the State of Niedersachsen/Germany for support of the construction of Advanced LIGO and construction and operation of the GEO600 detector. Additional support for Advanced LIGO was provided by the Australian Research Council. The authors gratefully acknowledge the Italian Istituto Nazionale di Fisica Nucleare (INFN), the French Centre National de la Recherche Scientifique (CNRS) and the Foundation for Fundamental Research on Matter supported by the Netherlands Organisation for Scientific Research, for the construction and operation of the Virgo detector and the creation and support of the EGO consortium. The authors also gratefully acknowledge research support from these agencies as well as by the Council of Scientific and Industrial Research of India, the Department of Science and Technology, India, the Science & Engineering Research Board (SERB), India, the Ministry of Human Resource Development, India, the Spanish Agencia Estatal de Investigación, the Vicepresidència i Conselleria d'Innovació Recerca i Turisme and the Conselleria d'Educació i Universitat del Govern de les Illes Balears, the Conselleria d'Educació Investigació Cultura i Esport de la Generalitat Valenciana, the National Science Centre of Poland, the Swiss National Science Foundation (SNSF), the Russian Foundation for Basic Research, the Russian Science Foundation, the European Commission, the European Regional Development Funds (ERDF), the Royal Society, the Scottish Funding Council, the Scottish Universities Physics Alliance, the Hungarian Scientific Research Fund (OTKA), the Lyon Institute of Origins (LIO), the National Research, Development and Innovation Office Hungary (NKFI), the National Research Foundation of Korea, Industry Canada and the Province of Ontario through the Ministry of Economic Development and Innovation, the Natural Science and Engineering Research Council Canada, the Canadian

Institute for Advanced Research, the Brazilian Ministry of Science, Technology, Innovations, and Communications, the International Center for Theoretical Physics South American Institute for Fundamental Research (ICTP-SAIFR), the Research Grants Council of Hong Kong, the National Natural Science Foundation of China (NSFC), the Leverhulme Trust, the Research Corporation, the Ministry of Science and Technology (MOST), Taiwan and the Kavli Foundation. The authors gratefully acknowledge the support of the NSF, STFC, MPS, INFN, CNRS, and the State of Niedersachsen/Germany for provision of computational resources.

References

Abbott, B. P., Abbott, R., Abbott, T. D., et al. 2016a, PhRvL, 116, 241102
Abbott, B. P., Abbott, R., Abbott, T. D., et al. 2016b, LRR, 19, 1
Abbott, B. P., Abbott, R., Abbott, T. D., et al. 2017a, Natur, 551, 85
Abbott, B. P., Abbott, R., Abbott, T. D., et al. 2017b, ApJL, 848, L13
Abbott, B. P., Abbott, R., Abbott, T. D., et al. 2017c, PhRvL, 119, 161101
Abbott, B. P., Abbott, R., Abbott, T. D., et al. 2017d, ApJL, 848, L12
Ade, P. A. R., Aghanim, N., Arnaud, M., et al. 2016, A&A, 594, A13
Akmal, A., Pandharipande, V. R., & Ravenhall, D. G. 1998, PhRvC, 58, 1804
Alexander, K. D., Berger, E., Fong, W., et al. 2017, ApJL, 848, L21
Antoniadis, J., Freire, P. C. C., Wex, N., et al. 2013, Sci, 340, 6131
Arcavi, I., Hosseinzadeh, G., Howell, D. A., et al. 2017, Natur, https://doi.org/10.1038/nature24291
Arnould, M., Goriely, S., & Takahashi, K. 2007, PhR, 450, 97
Barnes, J., & Kasen, D. 2013, ApJ, 775, 18
Barnes, J., Kasen, D., Wu, M.-R., & Martínez-Pinedo, G. 2016, ApJ, 829, 110
Bauswein, A., Goriely, S., & Janka, H.-T. 2013, ApJ, 773, 78
Beniamini, P., Hotokezaka, K., & Piran, T. 2016, ApJ, 832, 149
Bovard, L., Martin, D., Guercilena, F., et al. 2017, PhRvL, submitted (arXiv:1709.09630)
Buchdahl, H. A. 1959, PhRv, 116, 1027
Burbidge, E. M., Burbidge, G. R., Fowler, W. A., & Hoyle, F. 1957, RvMP, 29, 547
Burgay, M., D'Amico, N., Possenti, A., et al. 2003, Natur, 426, 531
Chornock, R., Berger, E., Kasen, D., et al. 2017, ApJL, 848, L19
Ciolfi, R., Kastaun, W., Giacomazzo, B., et al. 2017, PhRvD, 95, 063016
Côté, B., Belczynski, K., Fryer, C. L., et al. 2017, ApJ, 836, 230
Coughlin, M., Dietrich, T., Kawaguchi, K., et al. 2017, ApJ, 849, 12
Coulter, D. A., Foley, R. J., Kilpatrick, C. D., et al. 2017, Sci, https://doi.org/10.1126/science.aap9811
Covino, S., Wiersema, K., Fan, Y. Z., et al. 2017, NatAs, 1, 791
Cowperthwaite, P., Berger, E., Villar, V. A., et al. 2017, ApJL, 848, L17
Damour, T., Nagar, A., & Villain, L. 2012, PhRvD, 85, 123007
Del Pozzo, W., Li, T. G. F., Agathos, M., Van Den Broeck, C., & Vitale, S. 2013, PhRvL, 111, 071101
Demorest, P., Pennucci, T., Ransom, S., Roberts, M., & Hessels, J. 2010, Natur, 467, 1081
Dessart, L., Ott, C., Burrows, A., Rosswog, S., & Livne, E. 2009, ApJ, 690, 1681
Dessart, L., Ott, C. D., Burrows, A., Rosswog, S., & Livne, E. 2009, ApJ, 690, 1681
Diaz, M. C., Macri, L. M., Garcia Lambras, D., et al. 2017, ApJL, 848, L29
Dietrich, T., Bernuzzi, S., Ujevic, M., & Tichy, W. 2017a, PhRvD, 95, 044045
Dietrich, T., & Ujevic, M. 2017, CQGra, 34, 105014
Dietrich, T., Ujevic, M., Tichy, W., Bernuzzi, S., & Brügmann, B. 2017b, PhRvD, 95, 024029
Dominik, M., Belczynski, K., Fryer, C., et al. 2012, ApJ, 759, 52
Douchin, F., & Haensel, P. 2001, A&A, 380, 151
Drout, M. R., Piro, A. L., Shappee, B. J., et al. 2017, Sci, https://doi.org/10.1126/science.aaq0049
Endrizzi, A., Ciolfi, R., Giacomazzo, B., Kastaun, W., & Kawamura, T. 2016, CQGra, 33, 164001
Engvik, L., Bao, G., Hjorth-Jensen, M., Osnes, E., & Ostgaard, E. 1996, ApJ, 469, 794
Evans, P. A., Cenko, S. B., Kennea, J. A., et al. 2017, Sci, https://doi.org/10.1126/science.aap9580
Fernández, R., Kasen, D., Metzger, B. D., & Quataert, E. 2015, MNRAS, 446, 750
Foucart, F., O'Connor, E., Roberts, L., et al. 2016, PhRvD, 94, 123016
Freiburghaus, C., Rembges, J.-F., Rauscher, T., et al. 1999, ApJ, 516, 381
Fujibayashi, S., Sekiguchi, Y., Kiuchi, K., & Shibata, M. 2017, ApJ, 846, 114
Glendenning, N. K. 1985, ApJ, 293, 470
Goriely, S., Bauswein, A., & Janka, H.-T. 2011, ApJL, 738, L32
Goriely, S., Bauswein, A., Just, O., Pllumbi, E., & Janka, H.-T. 2015, MNRAS, 452, 3894
Flanagan, É. É., & Hinderer, T. 2008, PhRvD, 77, 021502
Hotokezaka, K., Kiuchi, K., Kyutoku, K., et al. 2013, PhRvD, 87, 024001
Ji, A. P., Frebel, A., Chiti, A., & Simon, J. D. 2016, Natur, 531, 610
Just, O., Bauswein, A., Pulpillo, R. A., Goriely, S., & Janka, H.-T. 2015, MNRAS, 448, 541
Kalogera, V., & Baym, G. 1996, ApJL, 470, L61
Kasen, D., Badnell, N. R., & Barnes, J. 2013, ApJ, 774, 25
Kasen, D., Fernandez, R., & Metzger, B. 2015, MNRAS, 450, 1777
Kasen, D., Metzger, B., Barnes, J., Quataert, E., & Ramirez-Ruiz, E. 2017, Natur, 551, 80
Kastaun, W., Ciolfi, R., Endrizzi, A., & Giacomazzo, B. 2017, PhRvD, 96, 043019
Kastaun, W., & Galeazzi, F. 2015, PhRvD, 91, 064027
Kawaguchi, K., Kyutoku, K., Shibata, M., & Tanaka, M. 2016, ApJ, 825, 52
Kiuchi, K., Sekiguchi, Y., Kyutoku, K., et al. 2015, PhRvD, 92, 064034
Lackey, B. D., Nayyar, M., & Owen, B. J. 2006, PhRvD, 73, 024021
Lattimer, J. M., & Prakash, M. 2001, ApJ, 550, 426
Lattimer, J. M., & Schramm, D. N. 1974, ApJL, 192, L145
Lehner, L., Liebling, S. L., Palenzuela, C., et al. 2016, CQGra, 33, 184002
Li, L.-X., & Paczynski, B. 1998, ApJL, 507, L59
Lipunov, V. N., Gorbovskoy, E., Kornilov, V. G., et al. 2017, ApJL, 850, L1
Lo, K.-W., & Lin, L.-M. 2011, ApJ, 728, 12
Madau, P., & Dickinson, M. 2014, ARA&A, 52, 415
Martin, D., Perego, A., Arcones, A., et al. 2015, ApJ, 813, 2
McCully, C., Hiramatsu, D., Howell, D. A., et al. 2017, ApJL, 848, L32
Metzger, B. D. 2017, LRR, 20, 3
Metzger, B. D., & Berger, E. 2012, ApJ, 746, 48
Metzger, B. D., & Fernandez, R. 2014, MNRAS, 441, 3444
Metzger, B. D., Martínez-Pinedo, G., Darbha, S., et al. 2010, MNRAS, 406, 2650
Müller, H., & Serot, B. D. 1996, NuPhA, 606, 508
Müther, H., Prakash, M., & Ainsworth, T. L. 1987, PhLB, 199, 469
Nakar, E. 2007, PhR, 442, 166
Nicholl, M., Berger, E., Kasen, D., et al. 2017, ApJL, 848, L18
O'Shaughnessy, R., Belczynski, K., & Kalogera, V. 2008, ApJ, 675, 566
Oertel, M., Hempel, M., Klähn, T., & Typel, S. 2017, RvMP, 89, 015007
Oppenheimer, J. R., & Volkoff, G. M. 1939, PhRv, 55, 374
Özel, F., & Freire, P. 2016, ARA&A, 54, 401
Perego, A., Rosswog, S., Cabezón, R. M., et al. 2014, MNRAS, 443, 3134
Pian, E., D'Avanzo, P., Bentti, S., et al. 2017, Natur, 551, 67
Qian, Y.-Z. 2000, ApJL, 534, L67
Radice, D., Galeazzi, F., Lippuner, J., et al. 2016, MNRAS, 460, 3255
Roberts, L. F., Kasen, D., Lee, W. H., & Ramirez-Ruiz, E. 2011, ApJL, 736, L21
Rosswog, S. 2013, RSPTA, 371, 20120272
Rosswog, S., Feindt, U., Korobkin, O., et al. 2017, CQGra, 34, 104001
Rosswog, S., Liebendörfer, M., Thielemann, F.-K., et al. 1999, A&A, 341, 499
Sekiguchi, Y., Kiuchi, K., Kyutoku, K., Shibata, M., & Taniguchi, K. 2016, PhRvD, 93, 124046
Shibata, M., Kiuchi, K., & Sekiguchi, Y.-I. 2017, PhRvD, 95, 083005
Siegel, D. M., & Metzger, B. D. 2017, PhRvL, in press (arXiv:1705.05473)
Smartt, S. J., Chen, T.-W., Jerkstrand, A., et al. 2017, Natur, 551, 75
Sneden, C., Cowan, J. J., & Gallino, R. 2008, ARA&A, 46, 241
Soares-Santos, M., Holz, D. E., Annis, J., et al. 2017, ApJL, 848, L16
Tanaka, M., & Hotokezaka, K. 2013, ApJ, 775, 113
Tanaka, M., Kato, D., Gaigalas, G., et al. 2017, arXiv:1708.09101
Tanaka, M., Utsumi, Y., Mazzali, P. A., et al. 2017, PASJ, psx121
Tanvir, N. R., Levan, A. J., González-Fernández, C., et al. 2017, ApJL, 848, L27
Terasawa, M., Sumiyoshi, K., Kajino, T., Mathews, G. J., & Tanihata, I. 2001, ApJ, 562, 470
Troja, E., Piro, L., van Eerten, H. J., et al. 2017, Natur, 551, 71
Valenti, S., Sand, D. J., Yang, S., et al. 2017, ApJL, 848, L24
Veitch, J., Raymond, V., Farr, B., et al. 2015, PhRvD, 91, 042003
Wade, L., Creighton, J. D. E., Ochsner, E., et al. 2014, PhRvD, 89, 103012
Wanajo, S., Sekiguchi, Y., Nishimura, N., et al. 2014, ApJL, 789, L39
Wiringa, R. B., Fiks, V., & Fabrocini, A. 1988, PhRvC, 38, 1010
Wollaeger, R. T., Korobkin, O., Fontes, C. J., et al. 2017, MNRAS, submitted (arXiv:1705.07084)
Yagi, K., & Yunes, N. 2017, PhR, 681, 1

B. P. Abbott[1], R. Abbott[1], T. D. Abbott[2], F. Acernese[3,4], K. Ackley[5,6], C. Adams[7], T. Adams[8], P. Addesso[9], R. X. Adhikari[1], V. B. Adya[10], C. Affeldt[10], M. Afrough[11], B. Agarwal[12], M. Agathos[13], K. Agatsuma[14], N. Aggarwal[15], O. D. Aguiar[16], L. Aiello[17,18], A. Ain[19], P. Ajith[20], B. Allen[10,21,22], G. Allen[12], A. Allocca[23,24], P. A. Altin[25], A. Amato[26], A. Ananyeva[1], S. B. Anderson[1], W. G. Anderson[21], S. V. Angelova[27], S. Antier[28], S. Appert[1], K. Arai[1], M. C. Araya[1], J. S. Areeda[29], N. Arnaud[28,30], K. G. Arun[31], S. Ascenzi[32,33], G. Ashton[10], M. Ast[34], S. M. Aston[7], P. Astone[35], D. V. Atallah[36], P. Aufmuth[22], C. Aulbert[10], K. AultONeal[37], C. Austin[2], A. Avila-Alvarez[29], S. Babak[38], P. Bacon[39], M. K. M. Bader[14], S. Bae[40], P. T. Baker[41], F. Baldaccini[42,43], G. Ballardin[30], S. Banagiri[44], J. C. Barayoga[1], S. E. Barclay[45], B. C. Barish[1], D. Barker[46], K. Barkett[47], F. Barone[3,4], B. Barr[45], L. Barsotti[15], M. Barsuglia[39], D. Barta[48], J. Bartlett[46], I. Bartos[5,49], R. Bassiri[50], A. Basti[23,24], J. C. Batch[46], M. Bawaj[43,51], J. C. Bayley[45], M. Bazzan[52,53], B. Bécsy[54], C. Beer[10], M. Bejger[55], I. Belahcene[28], A. S. Bell[45], G. Bergmann[10], S. Bernuzzi[56,57], J. J. Bero[58], C. P. L. Berry[59], D. Bersanetti[60], A. Bertolini[14], J. Betzwieser[7], S. Bhagwat[61], R. Bhandare[62], I. A. Bilenko[63], G. Billingsley[1], C. R. Billman[5], J. Birch[7], R. Birney[64], O. Birnholtz[10], S. Biscans[1,15], S. Biscoveanu[6,65], A. Bisht[22], M. Bitossi[24,30], C. Biwer[61], M. A. Bizouard[28], J. K. Blackburn[1], J. Blackman[47], C. D. Blair[1,66], D. G. Blair[66], R. M. Blair[46], S. Bloemen[67], O. Bock[10], N. Bode[10], M. Boer[68], G. Bogaert[68], A. Bohe[38], F. Bondu[69], E. Bonilla[50], R. Bonnand[8], B. A. Boom[14], R. Bork[1], V. Boschi[24,30], S. Bose[19,70], K. Bossie[7], Y. Bouffanais[39], A. Bozzi[30], C. Bradaschia[24], P. R. Brady[21], M. Branchesi[17,18], J. E. Brau[71], T. Briant[72], A. Brillet[68], M. Brinkmann[10], V. Brisson[28], P. Brockill[21], J. E. Broida[73], A. F. Brooks[1], D. D. Brown[74], S. Brunett[1], C. C. Buchanan[2], A. Buikema[15], T. Bulik[75], H. J. Bulten[14,76], A. Buonanno[38,77], D. Buskulic[8], C. Buy[39], R. L. Byer[50], M. Cabero[10], L. Cadonati[78], G. Cagnoli[26,79], C. Cahillane[1], J. Calderón Bustillo[78], T. A. Callister[1], E. Calloni[4,80], J. B. Camp[81], M. Canepa[60,82], P. Canizares[67], K. C. Cannon[83], H. Cao[74], J. Cao[84], C. D. Capano[10], E. Capocasa[39], F. Carbognani[30], S. Caride[85], M. F. Carney[86], J. Casanueva Diaz[28], C. Casentini[32,33], S. Caudill[14,21], M. Cavaglià[11], F. Cavalier[28], R. Cavalieri[30], G. Cella[24], C. B. Cepeda[1], P. Cerdá-Durán[87], G. Cerretani[23,24], E. Cesarini[33,88], S. J. Chamberlin[65], M. Chan[45], S. Chao[89], P. Charlton[90], E. Chase[91], E. Chassande-Mottin[39], D. Chatterjee[21], K. Chatziioannou[92], B. D. Cheeseboro[41], H. Y. Chen[93], X. Chen[66], Y. Chen[47], H.-P. Cheng[5], H. Chia[5], A. Chincarini[60], A. Chiummo[30], T. Chmiel[86], H. S. Cho[94], M. Cho[77], J. H. Chow[25], N. Christensen[68,73], Q. Chu[66], A. J. K. Chua[13], S. Chua[72], A. K. W. Chung[95], S. Chung[66], G. Ciani[5,52,53], R. Ciolfi[96,97], C. E. Cirelli[50], A. Cirone[60,82], F. Clara[46], J. A. Clark[78], P. Clearwater[98], F. Cleva[68], C. Cocchieri[11], E. Coccia[17,18], P.-F. Cohadon[72], D. Cohen[28], A. Colla[35,99], C. G. Collette[100], L. R. Cominsky[101], M. Constancio Jr.[16], L. Conti[53], S. J. Cooper[59], P. Corban[7], T. R. Corbitt[2], I. Cordero-Carrión[102], K. R. Corley[49], N. Cornish[103], A. Corsi[85], S. Cortese[30], C. A. Costa[16], M. W. Coughlin[1,73], S. B. Coughlin[91], J.-P. Coulon[68], S. T. Countryman[49], P. Couvares[1], P. B. Covas[104], E. E. Cowan[78], D. M. Coward[66], M. J. Cowart[7], D. C. Coyne[1], R. Coyne[85], J. D. E. Creighton[21], T. D. Creighton[105], J. Cripe[2], S. G. Crowder[106], T. J. Cullen[2,29], A. Cumming[45], L. Cunningham[45], E. Cuoco[30], T. Dal Canton[81], G. Dálya[54], S. L. Danilishin[10,22], S. D'Antonio[33], K. Danzmann[10,22], A. Dasgupta[107], C. F. Da Silva Costa[5], V. Dattilo[30], I. Dave[62], M. Davier[28], D. Davis[61], E. J. Daw[108], B. Day[78], S. De[61], D. DeBra[50], J. Degallaix[26], M. De Laurentis[4,17], S. Deléglise[72], W. Del Pozzo[23,24,59], N. Demos[15], T. Denker[10], T. Dent[10], R. De Pietri[56,57], V. Dergachev[38], R. De Rosa[4,80], R. T. DeRosa[7], C. De Rossi[26,30], R. DeSalvo[109], O. de Varona[10], J. Devenson[27], S. Dhurandhar[19], M. C. Díaz[105], T. Dietrich[38], L. Di Fiore[4], M. Di Giovanni[97,110], T. Di Girolamo[4,49,80], A. Di Lieto[23,24], S. Di Pace[35,99], I. Di Palma[35,99], F. Di Renzo[23,24], Z. Doctor[93], V. Dolique[26], F. Donovan[15], K. L. Dooley[11], S. Doravari[10], I. Dorrington[36], R. Douglas[45], M. Dovale Álvarez[59], T. P. Downes[21], M. Drago[10], C. Dreissigacker[10], J. C. Driggers[46], Z. Du[84], M. Ducrot[8], P. Dupej[45], S. E. Dwyer[46], T. B. Edo[108], M. C. Edwards[73], A. Effler[7], H.-B. Eggenstein[10,38], P. Ehrens[1], J. Eichholz[1], S. S. Eikenberry[5], R. A. Eisenstein[15], R. C. Essick[15], D. Estevez[8], Z. B. Etienne[41], T. Etzel[1], M. Evans[15], T. M. Evans[7], M. Factourovich[49], V. Fafone[17,32,33], H. Fair[61], S. Fairhurst[36], X. Fan[84], S. Farinon[60], B. Farr[93], W. M. Farr[59], E. J. Fauchon-Jones[36], M. Favata[111], M. Fays[36], C. Fee[86], H. Fehrmann[10], J. Feicht[1], M. M. Fejer[50], A. Fernandez-Galiana[15], I. Ferrante[23,24], E. C. Ferreira[16], F. Ferrini[30], F. Fidecaro[23,24], D. Finstad[61], I. Fiori[30], D. Fiorucci[39], M. Fishbach[93], R. P. Fisher[61], M. Fitz-Axen[44], R. Flaminio[26,112], M. Fletcher[45], H. Fong[92], J. A. Font[87,113], P. W. F. Forsyth[25], S. S. Forsyth[78], J.-D. Fournier[68], S. Frasca[35,99], F. Frasconi[24], Z. Frei[54], A. Freise[59], R. Frey[71], V. Frey[28], E. M. Fries[1], P. Fritschel[15], V. V. Frolov[7], P. Fulda[5], M. Fyffe[7], H. Gabbard[45], B. U. Gadre[19], S. M. Gaebel[59], J. R. Gair[114], L. Gammaitoni[42], M. R. Ganija[74], S. G. Gaonkar[19], C. Garcia-Quiros[104], F. Garufi[4,80], B. Gateley[46], S. Gaudio[37], G. Gaur[115], V. Gayathri[116], N. Gehrels[81,162], G. Gemme[60], E. Genin[30], A. Gennai[24], D. George[12], J. George[62], L. Gergely[117], V. Germain[8], S. Ghonge[78], Abhirup Ghosh[20], Archisman Ghosh[14,20], S. Ghosh[14,21,67], J. A. Giaime[2,7], K. D. Giardina[7], A. Giazotto[24], K. Gill[37], L. Glover[109], E. Goetz[118], R. Goetz[5], S. Gomes[36], B. Goncharov[6], G. González[2], J. M. Gonzalez Castro[23,24], A. Gopakumar[119], M. L. Gorodetsky[63], S. E. Gossan[1], M. Gosselin[30], R. Gouaty[8], A. Grado[4,120], C. Graef[45], M. Granata[26], A. Grant[45], S. Gras[15], C. Gray[46], G. Greco[121,122], A. C. Green[59], E. M. Gretarsson[37], P. Groot[67], H. Grote[10], S. Grunewald[38], P. Gruning[28], G. M. Guidi[121,122], X. Guo[84], A. Gupta[65], M. K. Gupta[107], K. E. Gushwa[1], E. K. Gustafson[1], R. Gustafson[118], O. Halim[17,18], B. R. Hall[70], E. D. Hall[15], E. Z. Hamilton[36], G. Hammond[45], M. Haney[123], M. M. Hanke[10], J. Hanks[46], C. Hanna[65], M. D. Hannam[36], O. A. Hannuksela[95], J. Hanson[7], T. Hardwick[2], J. Harms[17,18], G. M. Harry[124], I. W. Harry[38], M. J. Hart[45], C.-J. Haster[92], K. Haughian[45], J. Healy[58], A. Heidmann[72], M. C. Heintze[7], H. Heitmann[68], P. Hello[28], G. Hemming[30], M. Hendry[45], I. S. Heng[45], J. Hennig[45], A. W. Heptonstall[1], M. Heurs[10,22], S. Hild[45], T. Hinderer[67], D. Hoak[30], D. Hofman[26], K. Holt[7], D. E. Holz[93], P. Hopkins[36],

C. Horst[21], J. Hough[45], E. A. Houston[45], E. J. Howell[66], A. Hreibi[68], Y. M. Hu[10], E. A. Huerta[12], D. Huet[28], B. Hughey[37], S. Husa[104], S. H. Huttner[45], T. Huynh-Dinh[7], N. Indik[10], R. Inta[85], G. Intini[35,99], H. N. Isa[45], J.-M. Isac[72], M. Isi[1], B. R. Iyer[20], K. Izumi[46], T. Jacqmin[72], K. Jani[78], P. Jaranowski[125], S. Jawahar[64], F. Jiménez-Forteza[104], W. W. Johnson[2], N. K. Johnson-McDaniel[13], D. I. Jones[126], R. Jones[45], R. J. G. Jonker[14], L. Ju[66], J. Junker[10], C. V. Kalaghatgi[36], V. Kalogera[91], B. Kamai[1], S. Kandhasamy[7], G. Kang[40], J. B. Kanner[1], S. J. Kapadia[21], S. Karki[71], K. S. Karvinen[10], M. Kasprzack[2], W. Kastaun[10], M. Katolik[12], E. Katsavounidis[15], W. Katzman[7], S. Kaufer[22], K. Kawabe[46], K. Kawaguchi[38], F. Kéfélian[68], D. Keitel[45], A. J. Kemball[12], R. Kennedy[108], C. Kent[36], J. S. Key[127], F. Y. Khalili[63], I. Khan[17,33], S. Khan[10], Z. Khan[107], E. A. Khazanov[128], N. Kijbunchoo[25], Chunglee Kim[129], J. C. Kim[130], K. Kim[95], W. Kim[74], W. S. Kim[131], Y.-M. Kim[94], S. J. Kimbrell[78], E. J. King[74], P. J. King[46], M. Kinley-Hanlon[124], R. Kirchhoff[10], J. S. Kissel[46], L. Kleybolte[34], S. Klimenko[5], T. D. Knowles[41], P. Koch[10], S. M. Koehlenbeck[10], S. Koley[14], V. Kondrashov[1], A. Kontos[15], M. Korobko[34], W. Z. Korth[1], I. Kowalska[75], D. B. Kozak[1], C. Krämer[10], V. Kringel[10], A. Królak[132,133], G. Kuehn[10], P. Kumar[92], R. Kumar[107], S. Kumar[20], L. Kuo[89], A. Kutynia[132], S. Kwang[21], B. D. Lackey[38], K. H. Lai[95], M. Landry[46], R. N. Lang[134], J. Lange[58], B. Lantz[50], R. K. Lanza[15], S. L. Larson[91], A. Lartaux-Vollard[28], P. D. Lasky[6], M. Laxen[7], A. Lazzarini[1], C. Lazzaro[53], P. Leaci[35,99], S. Leavey[45], C. H. Lee[94], H. K. Lee[135], H. M. Lee[136], H. W. Lee[130], K. Lee[45], J. Lehmann[10], A. Lenon[41], M. Leonardi[97,110], N. Leroy[28], N. Letendre[8], Y. Levin[6], T. G. F. Li[95], S. D. Linker[109], T. B. Littenberg[137], J. Liu[66], X. Liu[21], R. K. L. Lo[95], N. A. Lockerbie[64], L. T. London[36], J. E. Lord[61], M. Lorenzini[17,18], V. Loriette[138], M. Lormand[7], G. Losurdo[24], J. D. Lough[10], C. O. Lousto[58], G. Lovelace[29], H. Lück[10,22], D. Lumaca[32,33], A. P. Lundgren[10], R. Lynch[15], Y. Ma[47], R. Macas[36], S. Macfoy[27], B. Machenschalk[10], M. MacInnis[15], D. M. Macleod[36], I. Magaña Hernandez[21], F. Magaña-Sandoval[61], L. Magaña Zertuche[61], R. M. Magee[65], E. Majorana[35], I. Maksimovic[138], N. Man[68], V. Mandic[44], V. Mangano[45], G. L. Mansell[25], M. Manske[21,25], M. Mantovani[30], F. Marchesoni[43,51], F. Marion[8], S. Márka[49], Z. Márka[49], C. Markakis[12], A. S. Markosyan[50], A. Markowitz[1], E. Maros[1], A. Marquina[102], F. Martelli[121,122], L. Martellini[68], I. W. Martin[45], R. M. Martin[111], D. V. Martynov[15], K. Mason[15], E. Massera[108], A. Masserot[8], T. J. Massinger[1], M. Masso-Reid[45], S. Mastrogiovanni[35,99], A. Matas[44], F. Matichard[1,15], L. Matone[49], N. Mavalvala[15], N. Mazumder[70], R. McCarthy[46], D. E. McClelland[25], S. McCormick[7], L. McCuller[15], S. C. McGuire[139], G. McIntyre[1], J. McIver[1], D. J. McManus[25], L. McNeill[6], T. McRae[25], S. T. McWilliams[41], D. Meacher[65], G. D. Meadors[10,38], M. Mehmet[10], J. Meidam[14], E. Mejuto-Villa[9], A. Melatos[98], G. Mendell[46], R. A. Mercer[21], E. L. Merilh[46], M. Merzougui[68], S. Meshkov[1], C. Messenger[45], C. Messick[65], R. Metzdorff[72], P. M. Meyers[44], H. Miao[59], C. Michel[26], H. Middleton[59], E. E. Mikhailov[140], L. Milano[4,80], A. L. Miller[5,35,99], B. B. Miller[91], J. Miller[15], M. Millhouse[103], M. C. Milovich-Goff[109], O. Minazzoli[68,141], Y. Minenkov[33], J. Ming[38], C. Mishra[142], S. Mitra[19], V. P. Mitrofanov[63], G. Mitselmakher[5], R. Mittleman[15], D. Moffa[86], A. Moggi[24], K. Mogushi[11], M. Mohan[30], S. R. P. Mohapatra[15], M. Montani[121,122], C. J. Moore[13], D. Moraru[46], G. Moreno[46], S. R. Morriss[105], B. Mours[8], C. M. Mow-Lowry[59], G. Mueller[5], A. W. Muir[36], Arunava Mukherjee[10], D. Mukherjee[21], S. Mukherjee[105], N. Mukund[19], A. Mullavey[7], J. Munch[74], E. A. Muñiz[61], M. Muratore[37], P. G. Murray[45], K. Napier[78], I. Nardecchia[32,33], L. Naticchioni[35,99], R. K. Nayak[143], J. Neilson[109], G. Nelemans[14,67], T. J. N. Nelson[7], M. Nery[10], A. Neunzert[118], L. Nevin[1], J. M. Newport[124], G. Newton[45,163], K. K. Y. Ng[95], T. T. Nguyen[25], D. Nichols[67], A. B. Nielsen[10], S. Nissanke[14,67], A. Nitz[10], A. Noack[10], F. Nocera[30], D. Nolting[7], C. North[36], L. K. Nuttall[36], J. Oberling[46], G. D. O'Dea[109], G. H. Ogin[144], J. J. Oh[131], S. H. Oh[131], F. Ohme[10], M. A. Okada[16], M. Oliver[104], P. Oppermann[10], Richard J. Oram[7], B. O'Reilly[7], R. Ormiston[44], L. F. Ortega[5], R. O'Shaughnessy[58], S. Ossokine[38], D. J. Ottaway[74], H. Overmier[7], B. J. Owen[85], A. E. Pace[65], J. Page[137], M. A. Page[66], A. Pai[116,145], S. A. Pai[62], J. R. Palamos[71], O. Palashov[128], C. Palomba[35], A. Pal-Singh[34], Howard Pan[89], Huang-Wei Pan[89], B. Pang[47], P. T. H. Pang[95], C. Pankow[91], F. Pannarale[36], B. C. Pant[62], F. Paoletti[24], A. Paoli[30], M. A. Papa[10,21,38], A. Parida[19], W. Parker[7], D. Pascucci[45], A. Pasqualetti[30], R. Passaquieti[23,24], D. Passuello[24], M. Patil[133], B. Patricelli[24,146], B. L. Pearlstone[45], M. Pedraza[1], R. Pedurand[26,147], L. Pekowsky[61], A. Pele[7], S. Penn[148], C. J. Perez[46], A. Perreca[1,97,110], L. M. Perri[91], H. P. Pfeiffer[38,92], M. Phelps[45], O. J. Piccinni[35,99], M. Pichot[68], F. Piergiovanni[121,122], V. Pierro[9], G. Pillant[30], L. Pinard[26], I. M. Pinto[9], M. Pirello[46], M. Pitkin[45], M. Poe[21], R. Poggiani[23,24], P. Popolizio[30], E. K. Porter[39], A. Post[10], J. Powell[45,149], J. Prasad[19], J. W. W. Pratt[37], G. Pratten[104], V. Predoi[36], T. Prestegard[21], M. Prijatelj[10], M. Principe[9], S. Privitera[38], G. A. Prodi[97,110], L. G. Prokhorov[63], O. Puncken[10], M. Punturo[43], P. Puppo[35], M. Pürrer[38], H. Qi[21], V. Quetschke[105], E. A. Quintero[1], R. Quitzow-James[71], D. S. Rabeling[25], H. Radkins[46], P. Raffai[54], S. Raja[62], C. Rajan[62], B. Rajbhandari[85], M. Rakhmanov[105], K. E. Ramirez[105], A. Ramos-Buades[104], P. Rapagnani[35,99], V. Raymond[38], M. Razzano[23,24], J. Read[29], T. Regimbau[68], L. Rei[60], S. Reid[64], D. H. Reitze[1,5], W. Ren[12], S. D. Reyes[61], F. Ricci[35,99], P. M. Ricker[12], S. Rieger[10], K. Riles[118], M. Rizzo[58], N. A. Robertson[1,45], R. Robie[45], F. Robinet[28], A. Rocchi[33], L. Rolland[8], J. G. Rollins[1], V. J. Roma[71], R. Romano[3,4], C. L. Romel[46], J. H. Romie[7], D. Rosińska[55,150], M. P. Ross[151], S. Rowan[45], A. Rüdiger[10], P. Ruggi[30], G. Rutins[27], K. Ryan[46], S. Sachdev[1], T. Sadecki[46], L. Sadeghian[21], M. Sakellariadou[152], L. Salconi[30], M. Saleem[116], F. Salemi[10], A. Samajdar[143], L. Sammut[6], L. M. Sampson[91], E. J. Sanchez[1], L. E. Sanchez[1], N. Sanchis-Gual[87], V. Sandberg[46], J. R. Sanders[61], B. Sassolas[26], O. Sauter[118], R. L. Savage[46], A. Sawadsky[34], P. Schale[71], M. Scheel[47], J. Scheuer[91], J. Schmidt[10], P. Schmidt[1,67], R. Schnabel[34], R. M. S. Schofield[71], A. Schönbeck[34], E. Schreiber[10], D. Schuette[10,22], B. W. Schulte[10], B. F. Schutz[10,36], S. G. Schwalbe[37], J. Scott[45], S. M. Scott[25], E. Seidel[12], D. Sellers[7], A. S. Sengupta[153], D. Sentenac[30], V. Sequino[17,32,33], A. Sergeev[128], D. A. Shaddock[25], T. J. Shaffer[46], A. A. Shah[137], M. S. Shahriar[91], M. B. Shaner[109], L. Shao[38], B. Shapiro[50], P. Shawhan[77],

A. Sheperd[21], D. H. Shoemaker[15], D. M. Shoemaker[78], K. Siellez[78], X. Siemens[21], M. Sieniawska[55], D. Sigg[46], A. D. Silva[16], L. P. Singer[81], A. Singh[10,22,38], A. Singhal[17,35], A. M. Sintes[104], B. J. J. Slagmolen[25], B. Smith[7], J. R. Smith[29], R. J. E. Smith[1,6], S. Somala[154], E. J. Son[131], J. A. Sonnenberg[21], B. Sorazu[45], F. Sorrentino[60], T. Souradeep[19], A. P. Spencer[45], A. K. Srivastava[107], K. Staats[37], A. Staley[49], M. Steinke[10], J. Steinlechner[34,45], S. Steinlechner[34], D. Steinmeyer[10], S. P. Stevenson[59,149], R. Stone[105], D. J. Stops[59], K. A. Strain[45], G. Stratta[121,122], S. E. Strigin[63], A. Strunk[46], R. Sturani[155], A. L. Stuver[7], T. Z. Summerscales[156], L. Sun[98], S. Sunil[107], J. Suresh[19], P. J. Sutton[36], B. L. Swinkels[30], M. J. Szczepańczyk[37], M. Tacca[14], S. C. Tait[45], C. Talbot[6], D. Talukder[71], D. B. Tanner[5], M. Tápai[117], A. Taracchini[38], J. D. Tasson[73], J. A. Taylor[137], R. Taylor[1], S. V. Tewari[148], T. Theeg[10], F. Thies[10], E. G. Thomas[59], M. Thomas[7], P. Thomas[46], K. A. Thorne[7], E. Thrane[6], S. Tiwari[17,97], V. Tiwari[36], K. V. Tokmakov[64], K. Toland[45], M. Tonelli[23,24], Z. Tornasi[45], A. Torres-Forné[87], C. I. Torrie[1], D. Töyrä[59], F. Travasso[30,43], G. Traylor[7], J. Trinastic[5], M. C. Tringali[97,110], L. Trozzo[24,157], K. W. Tsang[14], M. Tse[15], R. Tso[1], L. Tsukada[83], D. Tsuna[83], D. Tuyenbayev[105], K. Ueno[21], D. Ugolini[158], C. S. Unnikrishnan[119], A. L. Urban[1], S. A. Usman[36], H. Vahlbruch[22], G. Vajente[1], G. Valdes[2], N. van Bakel[14], M. van Beuzekom[14], J. F. J. van den Brand[14,76], C. Van Den Broeck[14,159], D. C. Vander-Hyde[61], L. van der Schaaf[14], J. V. van Heijningen[14], A. A. van Veggel[45], M. Vardaro[52,53], V. Varma[47], S. Vass[1], M. Vasúth[48], A. Vecchio[59], G. Vedovato[53], J. Veitch[45], P. J. Veitch[74], K. Venkateswara[151], G. Venugopalan[1], D. Verkindt[8], F. Vetrano[121,122], A. Viceré[121,122], A. D. Viets[21], S. Vinciguerra[59], D. J. Vine[27], J.-Y. Vinet[68], S. Vitale[15], T. Vo[61], H. Vocca[42,43], C. Vorvick[46], S. P. Vyatchanin[63], A. R. Wade[1], L. E. Wade[86], M. Wade[86], R. Walet[14], M. Walker[29], L. Wallace[1], S. Walsh[10,21,38], G. Wang[17,122], H. Wang[59], J. Z. Wang[65], W. H. Wang[105], Y. F. Wang[95], R. L. Ward[25], J. Warner[46], M. Was[8], J. Watchi[100], B. Weaver[46], L.-W. Wei[10,22], M. Weinert[10], A. J. Weinstein[1], R. Weiss[15], L. Wen[66], E. K. Wessel[12], P. Weßels[10], J. Westerweck[10], T. Westphal[10], K. Wette[25], J. T. Whelan[58], B. F. Whiting[5], C. Whittle[6], D. Wilken[10], D. Williams[45], R. D. Williams[1], A. R. Williamson[67], J. L. Willis[1,160], B. Willke[10,22], M. H. Wimmer[10], W. Winkler[10], C. C. Wipf[1], H. Wittel[10,22], G. Woan[45], J. Woehler[10], J. Wofford[58], K. W. K. Wong[95], J. Worden[46], J. L. Wright[45], D. S. Wu[10], D. M. Wysocki[58], S. Xiao[1], H. Yamamoto[1], C. C. Yancey[77], L. Yang[161], M. J. Yap[25], M. Yazback[5], Hang Yu[15], Haocun Yu[15], M. Yvert[8], A. Zadrożny[132], M. Zanolin[37], T. Zelenova[30], J.-P. Zendri[53], M. Zevin[91], L. Zhang[1], M. Zhang[140], T. Zhang[45], Y.-H. Zhang[58], C. Zhao[66], M. Zhou[91], Z. Zhou[91], S. J. Zhu[10,38], X. J. Zhu[6], A. B. Zimmerman[92], M. E. Zucker[1,15], and J. Zweizig[1]

(LIGO Scientific Collaboration and Virgo Collaboration)

[1] LIGO, California Institute of Technology, Pasadena, CA 91125, USA
[2] Louisiana State University, Baton Rouge, LA 70803, USA
[3] Università di Salerno, Fisciano, I-84084 Salerno, Italy
[4] INFN, Sezione di Napoli, Complesso Universitario di Monte S.Angelo, I-80126 Napoli, Italy
[5] University of Florida, Gainesville, FL 32611, USA
[6] OzGrav, School of Physics & Astronomy, Monash University, Clayton 3800, Victoria, Australia
[7] LIGO Livingston Observatory, Livingston, LA 70754, USA
[8] Laboratoire d'Annecy-le-Vieux de Physique des Particules (LAPP), Université Savoie Mont Blanc, CNRS/IN2P3, F-74941 Annecy, France
[9] University of Sannio at Benevento, I-82100 Benevento, Italy and INFN, Sezione di Napoli, I-80100 Napoli, Italy
[10] Max Planck Institute for Gravitational Physics (Albert Einstein Institute), D-30167 Hannover, Germany
[11] The University of Mississippi, University, MS 38677, USA
[12] NCSA, University of Illinois at Urbana-Champaign, Urbana, IL 61801, USA
[13] University of Cambridge, Cambridge CB2 1TN, UK
[14] Nikhef, Science Park, 1098 XG Amsterdam, The Netherlands
[15] LIGO, Massachusetts Institute of Technology, Cambridge, MA 02139, USA
[16] Instituto Nacional de Pesquisas Espaciais, 12227-010 São José dos Campos, São Paulo, Brazil
[17] Gran Sasso Science Institute (GSSI), I-67100 L'Aquila, Italy
[18] INFN, Laboratori Nazionali del Gran Sasso, I-67100 Assergi, Italy
[19] Inter-University Centre for Astronomy and Astrophysics, Pune 411007, India
[20] International Centre for Theoretical Sciences, Tata Institute of Fundamental Research, Bengaluru 560089, India
[21] University of Wisconsin-Milwaukee, Milwaukee, WI 53201, USA
[22] Leibniz Universität Hannover, D-30167 Hannover, Germany
[23] Università di Pisa, I-56127 Pisa, Italy
[24] INFN, Sezione di Pisa, I-56127 Pisa, Italy
[25] OzGrav, Australian National University, Canberra, Australian Capital Territory 0200, Australia
[26] Laboratoire des Matériaux Avancés (LMA), CNRS/IN2P3, F-69622 Villeurbanne, France
[27] SUPA, University of the West of Scotland, Paisley PA1 2BE, UK
[28] LAL, Univ. Paris-Sud, CNRS/IN2P3, Université Paris-Saclay, F-91898 Orsay, France
[29] California State University Fullerton, Fullerton, CA 92831, USA
[30] European Gravitational Observatory (EGO), I-56021 Cascina, Pisa, Italy
[31] Chennai Mathematical Institute, Chennai 603103, India
[32] Università di Roma Tor Vergata, I-00133 Roma, Italy
[33] INFN, Sezione di Roma Tor Vergata, I-00133 Roma, Italy
[34] Universität Hamburg, D-22761 Hamburg, Germany
[35] INFN, Sezione di Roma, I-00185 Roma, Italy
[36] Cardiff University, Cardiff CF24 3AA, UK
[37] Embry-Riddle Aeronautical University, Prescott, AZ 86301, USA
[38] Max Planck Institute for Gravitational Physics (Albert Einstein Institute), D-14476 Potsdam-Golm, Germany
[39] APC, AstroParticule et Cosmologie, Université Paris Diderot, CNRS/IN2P3, CEA/Irfu, Observatoire de Paris, Sorbonne Paris Cité, F-75205 Paris Cedex 13, France
[40] Korea Institute of Science and Technology Information, Daejeon 34141, Korea

[41] West Virginia University, Morgantown, WV 26506, USA
[42] Università di Perugia, I-06123 Perugia, Italy
[43] INFN, Sezione di Perugia, I-06123 Perugia, Italy
[44] University of Minnesota, Minneapolis, MN 55455, USA
[45] SUPA, University of Glasgow, Glasgow G12 8QQ, UK
[46] LIGO Hanford Observatory, Richland, WA 99352, USA
[47] Caltech CaRT, Pasadena, CA 91125, USA
[48] Wigner RCP, RMKI, H-1121 Budapest, Konkoly Thege Miklós út 29-33, Hungary
[49] Columbia University, New York, NY 10027, USA
[50] Stanford University, Stanford, CA 94305, USA
[51] Università di Camerino, Dipartimento di Fisica, I-62032 Camerino, Italy
[52] Università di Padova, Dipartimento di Fisica e Astronomia, I-35131 Padova, Italy
[53] INFN, Sezione di Padova, I-35131 Padova, Italy
[54] Institute of Physics, Eötvös University, Pázmány P. s. 1/A, Budapest 1117, Hungary
[55] Nicolaus Copernicus Astronomical Center, Polish Academy of Sciences, 00-716, Warsaw, Poland
[56] Dipartimento di Scienze Matematiche, Fisiche e Informatiche, Università di Parma, I-43124 Parma, Italy
[57] INFN, Sezione di Milano Bicocca, Gruppo Collegato di Parma, I-43124 Parma, Italy
[58] Rochester Institute of Technology, Rochester, NY 14623, USA
[59] University of Birmingham, Birmingham B15 2TT, UK
[60] INFN, Sezione di Genova, I-16146 Genova, Italy
[61] Syracuse University, Syracuse, NY 13244, USA
[62] RRCAT, Indore MP 452013, India
[63] Faculty of Physics, Lomonosov Moscow State University, Moscow 119991, Russia
[64] SUPA, University of Strathclyde, Glasgow G1 1XQ, UK
[65] The Pennsylvania State University, University Park, PA 16802, USA
[66] OzGrav, University of Western Australia, Crawley, Western Australia 6009, Australia
[67] Department of Astrophysics/IMAPP, Radboud University Nijmegen, P.O. Box 9010, 6500 GL Nijmegen, The Netherlands
[68] Artemis, Université Côte d'Azur, Observatoire Côte d'Azur, CNRS, CS 34229, F-06304 Nice Cedex 4, France
[69] Institut FOTON, CNRS, Université de Rennes 1, F-35042 Rennes, France
[70] Washington State University, Pullman, WA 99164, USA
[71] University of Oregon, Eugene, OR 97403, USA
[72] Laboratoire Kastler Brossel, UPMC-Sorbonne Universités, CNRS, ENS-PSL Research University, Collège de France, F-75005 Paris, France
[73] Carleton College, Northfield, MN 55057, USA
[74] OzGrav, University of Adelaide, Adelaide, South Australia 5005, Australia
[75] Astronomical Observatory Warsaw University, 00-478 Warsaw, Poland
[76] VU University Amsterdam, 1081 HV Amsterdam, The Netherlands
[77] University of Maryland, College Park, MD 20742, USA
[78] Center for Relativistic Astrophysics, Georgia Institute of Technology, Atlanta, GA 30332, USA
[79] Université Claude Bernard Lyon 1, F-69622 Villeurbanne, France
[80] Università di Napoli "Federico II," Complesso Universitario di Monte S.Angelo, I-80126 Napoli, Italy
[81] NASA Goddard Space Flight Center, Greenbelt, MD 20771, USA
[82] Dipartimento di Fisica, Università degli Studi di Genova, I-16146 Genova, Italy
[83] RESCEU, University of Tokyo, Tokyo, 113-0033, Japan
[84] Tsinghua University, Beijing 100084, China
[85] Texas Tech University, Lubbock, TX 79409, USA
[86] Kenyon College, Gambier, OH 43022, USA
[87] Departamento de Astronomía y Astrofísica, Universitat de València, E-46100 Burjassot, València, Spain
[88] Museo Storico della Fisica e Centro Studi e Ricerche Enrico Fermi, I-00184 Roma, Italy
[89] National Tsing Hua University, Hsinchu City, 30013, Taiwan, Republic of China
[90] Charles Sturt University, Wagga Wagga, New South Wales 2678, Australia
[91] Center for Interdisciplinary Exploration & Research in Astrophysics (CIERA), Northwestern University, Evanston, IL 60208, USA
[92] Canadian Institute for Theoretical Astrophysics, University of Toronto, Toronto, Ontario M5S 3H8, Canada
[93] University of Chicago, Chicago, IL 60637, USA
[94] Pusan National University, Busan 46241, Korea
[95] The Chinese University of Hong Kong, Shatin, NT, Hong Kong
[96] INAF, Osservatorio Astronomico di Padova, I-35122 Padova, Italy
[97] INFN, Trento Institute for Fundamental Physics and Applications, I-38123 Povo, Trento, Italy
[98] OzGrav, University of Melbourne, Parkville, Victoria 3010, Australia
[99] Università di Roma "La Sapienza," I-00185 Roma, Italy
[100] Université Libre de Bruxelles, Brussels B-1050, Belgium
[101] Sonoma State University, Rohnert Park, CA 94928, USA
[102] Departamento de Matemáticas, Universitat de València, E-46100 Burjassot, València, Spain
[103] Montana State University, Bozeman, MT 59717, USA
[104] Universitat de les Illes Balears, IAC3—IEEC, E-07122 Palma de Mallorca, Spain
[105] The University of Texas Rio Grande Valley, Brownsville, TX 78520, USA
[106] Bellevue College, Bellevue, WA 98007, USA
[107] Institute for Plasma Research, Bhat, Gandhinagar 382428, India
[108] The University of Sheffield, Sheffield S10 2TN, UK
[109] California State University, Los Angeles, 5151 State University Dr, Los Angeles, CA 90032, USA
[110] Università di Trento, Dipartimento di Fisica, I-38123 Povo, Trento, Italy
[111] Montclair State University, Montclair, NJ 07043, USA
[112] National Astronomical Observatory of Japan, 2-21-1 Osawa, Mitaka, Tokyo 181-8588, Japan
[113] Observatori Astronòmic, Universitat de València, E-46980 Paterna, València, Spain
[114] School of Mathematics, University of Edinburgh, Edinburgh EH9 3FD, UK
[115] University and Institute of Advanced Research, Koba Institutional Area, Gandhinagar Gujarat 382007, India

[116] IISER-TVM, CET Campus, Trivandrum Kerala 695016, India
[117] University of Szeged, Dóm tér 9, Szeged 6720, Hungary
[118] University of Michigan, Ann Arbor, MI 48109, USA
[119] Tata Institute of Fundamental Research, Mumbai 400005, India
[120] INAF, Osservatorio Astronomico di Capodimonte, I-80131, Napoli, Italy
[121] Università degli Studi di Urbino "Carlo Bo," I-61029 Urbino, Italy
[122] INFN, Sezione di Firenze, I-50019 Sesto Fiorentino, Firenze, Italy
[123] Physik-Institut, University of Zurich, Winterthurerstrasse 190, 8057 Zurich, Switzerland
[124] American University, Washington, DC 20016, USA
[125] University of Białystok, 15-424 Białystok, Poland
[126] University of Southampton, Southampton SO17 1BJ, UK
[127] University of Washington Bothell, 18115 Campus Way NE, Bothell, WA 98011, USA
[128] Institute of Applied Physics, Nizhny Novgorod, 603950, Russia
[129] Korea Astronomy and Space Science Institute, Daejeon 34055, Korea
[130] Inje University Gimhae, South Gyeongsang 50834, Korea
[131] National Institute for Mathematical Sciences, Daejeon 34047, Korea
[132] NCBJ, 05-400 Świerk-Otwock, Poland
[133] Institute of Mathematics, Polish Academy of Sciences, 00656 Warsaw, Poland
[134] Hillsdale College, Hillsdale, MI 49242, USA
[135] Hanyang University, Seoul 04763, Korea
[136] Seoul National University, Seoul 08826, Korea
[137] NASA Marshall Space Flight Center, Huntsville, AL 35811, USA
[138] ESPCI, CNRS, F-75005 Paris, France
[139] Southern University and A&M College, Baton Rouge, LA 70813, USA
[140] College of William and Mary, Williamsburg, VA 23187, USA
[141] Centre Scientifique de Monaco, 8 quai Antoine Ier, MC-98000, Monaco
[142] Indian Institute of Technology Madras, Chennai 600036, India
[143] IISER-Kolkata, Mohanpur, West Bengal 741252, India
[144] Whitman College, 345 Boyer Avenue, Walla Walla, WA 99362 USA
[145] Indian Institute of Technology Bombay, Powai, Mumbai, Maharashtra 400076, India
[146] Scuola Normale Superiore, Piazza dei Cavalieri 7, I-56126 Pisa, Italy
[147] Université de Lyon, F-69361 Lyon, France
[148] Hobart and William Smith Colleges, Geneva, NY 14456, USA
[149] OzGrav, Swinburne University of Technology, Hawthorn VIC 3122, Australia
[150] Janusz Gil Institute of Astronomy, University of Zielona Góra, 65-265 Zielona Góra, Poland
[151] University of Washington, Seattle, WA 98195, USA
[152] King's College London, University of London, London WC2R 2LS, UK
[153] Indian Institute of Technology, Gandhinagar Ahmedabad Gujarat 382424, India
[154] Indian Institute of Technology Hyderabad, Sangareddy, Khandi, Telangana 502285, India
[155] International Institute of Physics, Universidade Federal do Rio Grande do Norte, Natal RN 59078-970, Brazil
[156] Andrews University, Berrien Springs, MI 49104, USA
[157] Università di Siena, I-53100 Siena, Italy
[158] Trinity University, San Antonio, TX 78212, USA
[159] Van Swinderen Institute for Particle Physics and Gravity, University of Groningen, Nijenborgh 4, 9747 AG Groningen, The Netherlands
[160] Abilene Christian University, Abilene, TX 79699, USA
[161] Colorado State University, Fort Collins, CO 80523, USA
[162] Deceased, 2017 February.
[163] Deceased, 2016 December.